Acta Biologica Szegediensis

Volume 70(1):54-63, 2026
Acta Biologica Szegediensis
http://abs.bibl.u-szeged.hu/index.php/abs
DOI:10.14232/abs.2026.1.54-63

ARTICLE

Anatomical and Endophytic Fungal Associations in *Christisonia tubulosa* (Wight) Benth. ex Hook.f. (Orobanchaceae)

Selvaraj Deepika*, Mayakrishnan Balachandar, Jayasankar Kalaiyarasan, Thangavelu Muthukumar

Root and Soil Biology Laboratory, Department of Botany, Bharathiar University, Coimbatore - 641046, Tamil Nadu, India

ABSTRACT *Christisonia tubulosa* (Wight) Benth. ex Hook.f. (Orobanchaceae) is a rare holoparasitic angiosperm distributed in the moist deciduous forests of the Western Ghats, India. The present study documents the vegetative anatomical characteristics and root-associated fungal structures of this species. Anatomical assessments were conducted on the scape, rootstock, and roots using light microscopy and scanning electron microscopy. The scape exhibited a single-layered epidermis, cortex, sclerenchymatous tissue, vascular bundles, and water-storage cells. The rootstock showed a compact epidermal layer, parenchymatous ground tissue, a vascular cylinder, starch grains, and raphides. The root system lacked root hairs, and haustorial attachment to the host root was observed. Fungal observations revealed colonization of the root cortex by hyphae, hyphal coils, and vesicle-like structures resembling those of arbuscular mycorrhizal fungi, as well as septate melanized hyphae, moniliform hyphae, and microsclerotia characteristic of dark septate endophytic fungi. Quantitative assessment showed significant variation in the extent of the observed fungal structures. This study provides a modern anatomical description of the vegetative organs and morphological documentation of root-associated fungal structures in the studied population of *C. tubulosa*.

KEY WORDS
Christisonia tubulosa
dark septate endophytes
haustorium
holoparasitic plant
Orobanchaceae
vegetative anatomy

ARTICLE INFORMATION
Submitted
11 April 2026
Accepted
29 June 2026
***Corresponding author**
E-mail: deepikaraj343@gmail.com

Introduction

Parasitic angiosperms have repeatedly lost photosynthesis and evolved specialized organs to procure water and carbon from hosts, making them excellent models for plant–plant interactions (Mutuku et al. 2021; Yoshida et al. 2016). The family *Orobanchaceae* represents a diverse lineage of parasitic and non-parasitic angiosperms that exhibit a broad range of trophic adaptations, from autotrophy to obligate parasitism, encompassing approximately 90–100 genera and over 2000 species worldwide (McNeal et al. 2013). Members of *Orobanchaceae* are characterized morphologically by the formation of haustorial connections to host roots, reduction or loss of vegetative structures in holoparasites, bilabiate zygomorphic flowers, and the production of numerous minute seeds within dehiscent capsules, all of which facilitate parasitic establishment and dispersal (Schneeweiss 2013; Goyet et al. 2019). *Christisonia tubulosa* (Wight) Benth. ex Hook.f. is a holoparasitic taxon that entirely lacks chlorophyll and derives its nutrition from host roots through haustorial connections (Thazhe et al. 2025; Mutuku et al. 2021). This taxon has a homotypic (*Oligopholis tubulosa* Wight) and a heterotypic (*Christisonia keralensis* Erady) synonym (POWO 2025). The Western Ghats of India are recognized as a centre of diversity for *Christisonia*, where *C. tubulosa* occurs in moist evergreen and montane forests of Kerala and Tamil Nadu (van Der Ent and Wong 2015). Its distribution is highly localized, usually confined to intact forest floors with high humidity (Thazhe et al. 2025). Discoveries of congeners such as *Christisonia mira* J. Mathew, *Christisonia flavirubens* J. Mathew & P.M. Salim, and *Christisonia rarissima* Rajendran & I. Kanivalan highlight the richness of the genus and suggest ecological overlap in the Southern Western Ghats (Jose and George 2015; Mathew and Salim 2022; Kanivalan and Rajendran 2022). These records also emphasize broader biogeographic links across South and Southeast Asia (Jose and George 2015).

Morphologically, *C. tubulosa* shows the reduction syndrome typical of holoparasites, underground vegetative tissues are fleshy and reduced, while the conspicuous aboveground structures are its tubular flowers (Thazhe et al. 2025; Mutuku et al. 2021). The calyx is persistent and accrescent, a diagnostic trait in Orobanchaceae (Bennett and Mathews 2006). The floral tube and sticky surface aid pollinator interaction and protect emerging tissues from litter and moisture stress (Thazhe et al. 2025; Jose and George 2015). Flowering is usually synchronized

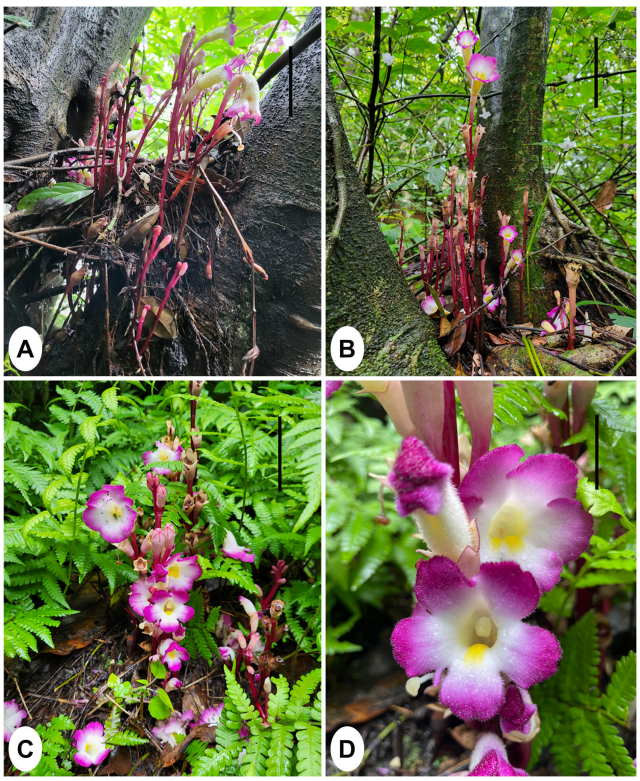

Figure 1. Habit of *Christisonia tubulosa* (A and B); Inflorescence (C and D). Scale bars = 5 cm

with monsoonal rains, enabling periodic emergence from the forest floor (Jose and George 2015). At the anatomical level, the haustorium is the defining organ for host attachment and vascular integration (Mutuku et al. 2021; Yoshida et al. 2016; Worsdell 1895). Haustorial initiation depends on host-derived signals such as quinones, cytokinins, and strigolactones, which regulate germination and invasive growth (Baskin and Baskin 2022; Furuta et al. 2021). Molecular studies in Orobanchaceae have revealed conserved transcriptional pathways and cell wall modifications that enable penetration and xylem connectivity (Yoshida et al. 2016; Mutuku et al. 2021). Pharmacognostic interest in Orobanchaceae stems from their unique secondary metabolites and bioactive potential (Goyet et al. 2019; Casadesús and Munné-Bosch 2021). While *C. tubulosa* remains poorly profiled chemically, related genera have yielded compounds with antioxidant and antimicrobial properties (Casadesús and Munné-Bosch 2021). Due to its rarity, research requires ethical sampling protocols and, where possible, *ex situ* conservation (Thazhe et al. 2025).

Although detailed investigations on *C. tubulosa* are limited, the present study reveals that the vegetative organs of this plant possess distinctive structural adaptations (Masumoto et al. 2021). These anatomical features elucidate the mechanisms by which *C. tubulosa* achieves physiological integration with its host plants despite the absence of chlorophyll (Thazhe et al. 2025). Due to the seasonal emergence of reproductive structures, the plant remains in a vegetative state during most part of the year, making identification challenging in natural conditions (Thazhe et al. 2025). Vegetative and anatomical markers of Orobanchaceae, such as the morphology of scape, cortical tissue organization, and haustorial architecture serve as reliable diagnostic traits for the recognition of this species during its vegetative phase (Mutuku et al. 2021). These markers not only support accurate species determination, but also contribute to a broader understanding of functional adaptations in holoparasitic taxa (Masumoto et al. 2021).

Roots of terrestrial plants are commonly associated with mycorrhizal fungi and dark septate endophytic (DSE) fungi, both of which enhance plant growth and survival. These fungi improve water and nutrient uptake and provide protection against various biotic and abiotic stresses (Ruotsalainen et al. 2022; Chaudhary et al. 2025). While non-mycorrhizal endophytic fungal associations have been observed in holoparasitic plants (Ikeda et al. 2016; Wu et al. 2022; Molina et al. 2024), instances of mycorrhizal or DSE fungal symbiosis in these plants are rare (De Vega et al. 2010; Brundrett 2011). De Vega et al. (2010) speculated that the presence of fungal hyphae, hyphal coils, and vesicles resembling those of arbuscular mycorrhizal (AM) fungi within endophytic tissues of the holoparasitic *Cytinus*, might enhance mineral uptake enhancing the fitness and successful parasitism of the holoparasite. We hypothesized that such tripartite interactions among endophytic fungi, holoparasite, and host can be crucial for the establishment and ecological success of *C. tubulosa* in nutrient-poor forest soils. Therefore, the present study focuses on the anatomy, and endophytic fungal colonization of the plant *C. tubulosa* occurring in the Western Ghats region of southern India.

Materials and Methods

Sample collection

The scape, root, and rootstock of *C. tubulosa* (Fig. 1) were collected from 10 plants during the monsoon season of 2024 at Valparai, located in the Anamalai Hills of the Western Ghats, Tamil Nadu, India (latitude: 10.39432°; longitude: 76.99208°; altitude: 1,193 m a.s.l). The plant specimen of *C. tubulosa* collected during the flowering phase, was authenticated by the Botanical Survey of India (BSI), Southern Circle, Coimbatore, India and the voucher specimen was deposited in the BHARATI Herbarium (008864), Department of Botany, Bharathiar University,

Coimbatore, India. The host specimen *Oreocnide integrifolia* (Gaudich.) Miq., was also collected and authenticated by the BSI, Southern Circle, Coimbatore, India. The anatomical features of the vegetative parts were examined, which included the scape, root, and rootstock. After collection, the plant materials were washed with distilled water and preserved in FAA (formalin–acetic acid in 70% ethanol) solution until further processing.

Determination of vegetative anatomy and microscopic analysis

The preserved vegetative materials of *C. tubulosa*, were subjected to free-hand sectioning using sharp razor blades (transverse sections, 25–30 µm) and were stained using safranin. The staining solution was prepared by mixing 50 mL of 2-methoxy ethanol with 25 mL of 100% ethanol. To this mixture, 25 mL of 37% formaldehyde was added. Finally, 1 g of safranin was added to the above solution, resulting in 1% w/v safranin. The staining solution was used after being filtered using Whatman No. 1 filter paper. Generally, for scapes, sections were taken 5 cm from the tip; and for roots, and rootstock, sections were made 5 cm from the tip. Then the anatomical parameters like the size or cell dimensions were measured (n=50) for the scape (epidermis, hypodermis, sclerenchymatous fibre, xylem, and water-storage cells), rootstock (epidermis, ground tissue, sclerenchymatous fibre, xylem, and water-storage cells), roots (epidermis, cortex, endodermis, xylem, and water-storage cells) using a calibrated ocular micrometer. Images of the sections were photographed using a ProgRes3 camera attached to an Olympus BX 51 light microscope.

Endophytic fungal colonization

For estimation of fungal colonization, the roots were cut into 1 cm long bits, cleared by boiling in 25% KOH at 100 °C for 60 min. The cleared roots were washed and treated with 5 N HCl for 30 min. The acidified roots were stained by placing them in trypan blue (0.05%, w/v) solution overnight (Koske and Gemma 1989). Squashes of stained root bits were prepared and observed for the presence of fungal structures. The magnified intersection method of McGonigle et al. (1990) was used to calculate the percentage of total root length colonization and root length containing different fungal structures like broad aseptate hyphae, hyphal coils, arbuscules, arbusculate coils, and vesicles for AM-like fungal colonization and melanized regularly septate hyphae, moniliform hyphae, and microsclerotia for DSE fungal colonization (McGonigle et al. 1990).

Scanning Electron Microscopy (SEM)

Transverse sections (~5 mm^2) of plant vegetative structures were examined using a SEM (VEGA3, TESCAN, Czech Republic) at 5.0 kV accelerating voltage with a working distance of 9.50–15.40 mm. Samples were mounted on aluminium stubs with carbon-conductive tape, sputter-coated with gold for 105 s, to improve surface conductivity. The specimens were then observed at magnifications ranging from ×20 to ×500.

Statistical analysis

Data on cell dimensions of epidermis, cortex, fibre, xylem, water-storage cells, and endophytic variables were subjected to one-way ANOVA after confirming homogeneity of variances through Levene's test. Mean comparisons were carried out using Duncan's multiple range test (DMRT) at a significance level of $P < 0.05$. All analyses were performed using Statistical Product and Service Solutions software (version 21.0).

Results

Scape

The scape consists of epidermis, hypodermis, sclerenchymatous fibres, xylem, and water-storage cells, exhibiting well-differentiated tissues with distinct tissue zones. The outermost epidermis is composed of a single layer of

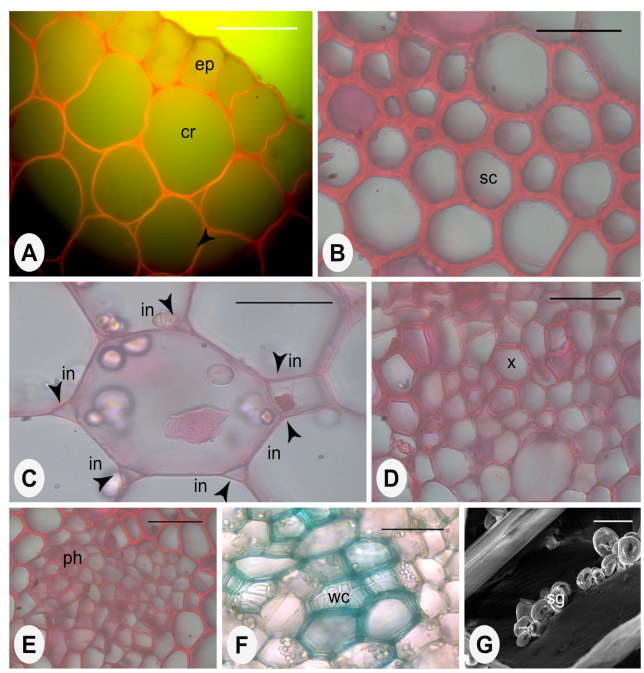

Figure 2. Transverse section of *Christisonia tubulosa* scape showing thin walled single-layered epidermis (ep), and cortex (cr) (A); sclerenchymatous cell (sc) (B); triangle and rectangle shaped intracellular spaces (black arrow heads) in the cortex (C); xylem (x) (D); phloem (ph) (E); water-storage cell (wc) present in cortical layer (F); scanning electron microscopic view of starch grains (sg) (G). Scale bars = 50 µm.

Table 1. Comparison of cell dimensions of *Christisonia tubulosa* scape, rootstock, and root in transverse section

Characters (µm)	Scape	Rootstock	Root	Statistics	
				Df	#F / ##t-value
Epidermis cell					
Length	21.95±0.41[b]	13.40±0.27[c]	25.50±1.16a	2,149	#72.896***
Width	30.20±0.58[b]	29.75±1.38[b]	37.10±1.46[a]	2,149	#11.707***
Wall thickness	3.45±0.19[a]	2.75±0.11[b]	2.65±0.08[b]	2,149	#10.590***
Cortex cell					
Length	--	--	50.65±1.12	--	--
Width	--	--	59.65±1.91	--	--
Hypodermis cell					
Length	67.15±0.88	--	--	--	--
Width	82.55±1.14	--	--	--	--
Ground tissue cell					
Length	--	64.60±1.34	--	--	--
Width	--	73.50±1.46	--	--	--
Endodermis cell					
Length	--	--	22.70±1.02	--	--
Width	--	--	38.40±1.19	--	--
Cell wall thickness	--	--	5.25±0.13		
Sclerenchymatous cell					
Length	77.20±1.45	--	54.25±1.22	49	##12.529***
Width	54.45±1.51	--	77.25±1.81	49	##-8.741***
Xylem cell					
Length	20.60±0.92[b]	23.75±0.80[a]	24.25±0.82[a]	2,149	#5.404**
Width	27.15±0.72[b]	30.65±1.11[a]	27.60±0.88[b]	2,149	#4.283*
Water-storage cell					
Length	28.95±0.84[a]	28.20±0.66[a]	27.45±0.68[a]	2,149	#1.048ns
Width	36.85±1.04[a]	35.60±0.80[ab]	33.15±1.15[b]	2,149	#3.500*

*, **, ***, and ns: Significant at P < 0.05, P < 0.01, P < 0.001, and not significant, respectively. Means ± S.E. in a row followed by the same letter(s) are not significantly different according to t-test (two-organ comparisons) or Duncan's Multiple Range Test (three-organ comparisons).

small and compact cells. All the quantitatively measured cellular variables significantly varied in the scape (Table 1). The epidermal cells measured 21.95 ± 0.41 µm in length, and 30.20 ± 0.58 µm in width, and possessed moderately thickened outer walls 3.45 ± 0.19 µm (Fig. 2A). Underlying the epidermis, the cortex is 8–15 layered consisting of large, thin-walled parenchymatous cells. These cortical cells had a mean length 67.15 ± 0.88 µm, and a width of 82.55 ± 1.14 µm (Fig. 2A). In transverse sections a well-developed sclerenchymatous zone was observed beneath the cortex, consisting of cells averaging 77.20±1.45 µm in length, and 54.45 ± 1.51 µm in width (Fig. 2B). The phloem was well developed, while the xylem elements were comparatively smaller and fewer in number, with cell dimension of 20.60 ± 0.92 µm in length, and 27.15 ± 0.72 µm in width (Fig. 2C-E). Prominently developed water-storage cells were also observed, measuring 28.95 ±0.84 µm in length, and 36.85 ± 1.04 µm in width (Fig. 2F). Numerous starch grains were observed within the cells, staining deep blue when treated with iodine (Fig. 2G).

Rootstock

The rootstock is cylindrical and brown. It consists of epidermis, cortex, sclerenchymatous tissue, xylem, and water-storage cells. The quantitatively measured cellular variables showed significant variation within the rootstock (Table 1). The epidermis is composed of small, compact cells measuring 13.40 ± 0.27 µm in length, and 29.75 ± 1.38 µm in width, with a cell wall thickness of 2.75 ± 0.11 µm (Fig. 3A). Beneath the epidermis, the ground tissue is broad and parenchymatous, consisting of large, thin-walled cells. These cells measure 64.60 ± 1.34 µm in length and 73.50 ± 1.46 µm in width with no intercellular spaces (Fig. 3A). The vascular tissue is embedded within the ground tissue and consists of relatively few xylem elements. The xylem cells measured 23.75 ± 0.80 µm in length and 30.65 ± 1.11 µm in width (Fig. 3B&C). The xylem and phloem were surrounded by pitted and banded water-storage

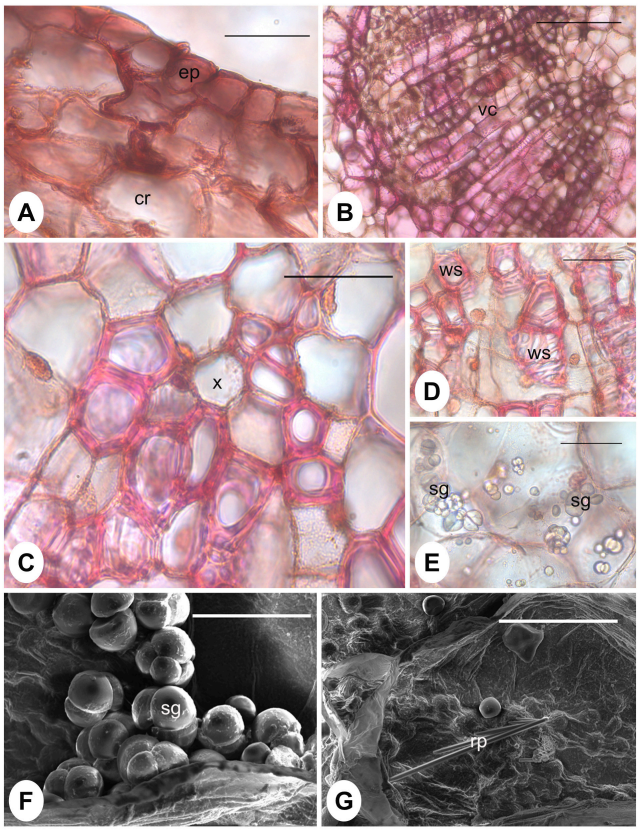

Figure 3. Transverse section of *Christisonia tubulosa* rootstock showing single-layered epidermis (ep), and cortex (cr) (A); vascular cylinder (vc) (B); xylem (x) (C); water-storage cells (wc) present in the stelar region (D); starch grains (sg) observed in cortical region (E); scanning electron microscope view of starch grains (sg) (F) and raphides (rp) (G). Scale bars = 50 µm.

cells. These water-storage cells measured 28.20 ± 0.66 µm in length, and 35.60 ± 0.80 µm in width (Fig. 3D). Also, there were raphides and numerous starch grains in the cells that stained deep blue with iodine (Fig. 3E-G).

Root

Roots are well developed and show a distinct radial organization with clearly differentiated outer and inner tissues. In transverse section, the root exhibits a compact peripheral region enclosing a broad parenchymatous cortex and a well-defined stele. Root hairs were absent. The epidermis is uniseriate and composed of compact cells measuring 25.50 ± 1.16 µm in length, and 37.10 ± 1.46 µm in width (Fig. 4A). The epidermal cell walls show marked thickening, with an average thickness of 2.65 ± 0.08 µm (Fig. 4A). Subtending the epidermis, the cortex is broad and parenchymatous, consisting of 8–10 layers of large cells. Cortical cells are polygonal to round in outline and measure 50.65 ± 1.12 µm in length, and 59.65 ± 1.91 µm in width (Fig. 4A). Endodermal cells measure 22.70 ± 1.02 µm in length, and 38.40 ± 1.19 µm in width, and exhibit prominent cell wall thickening (5.25 ± 0.13 µm) (Fig. 4B). The endodermis and pericycle are indistinguishable. Within the stele, sclerenchymatous tissue is well developed and occurs as discrete strands. The sclerenchymatous cells were thick-walled, measuring 54.25 ± 1.22 µm in length, and 77.25 ± 1.81 µm in width. The xylem is composed of comparatively small elements arranged compactly, with individual elements measuring 24.25 ± 0.82 µm in length and 27.60 ± 0.88 µm in width (Fig. 4B). Water-storage cells are present in association with the vascular tissues, measuring 27.45 ± 0.68 µm in length and 33.15 ± 1.15 µm in width (Fig. 4C). Furthermore, abundant starch grains were present within the cells, staining deep blue colour in iodine (Fig. 4D-F). The haustorium connection between the infected root portions of the host plant *O. integrifolia* associated with *C. tubulosa* roots, is shown in Fig. 5.

Fungal colonization

The fungal colonization in the roots of *C. tubulosa* was observed as linear broad aseptate hyphae, hyphal coils, and vesicles (Fig. 6). The occurrence of dark septate hyphae, moniliform hyphae, and microsclerotia were

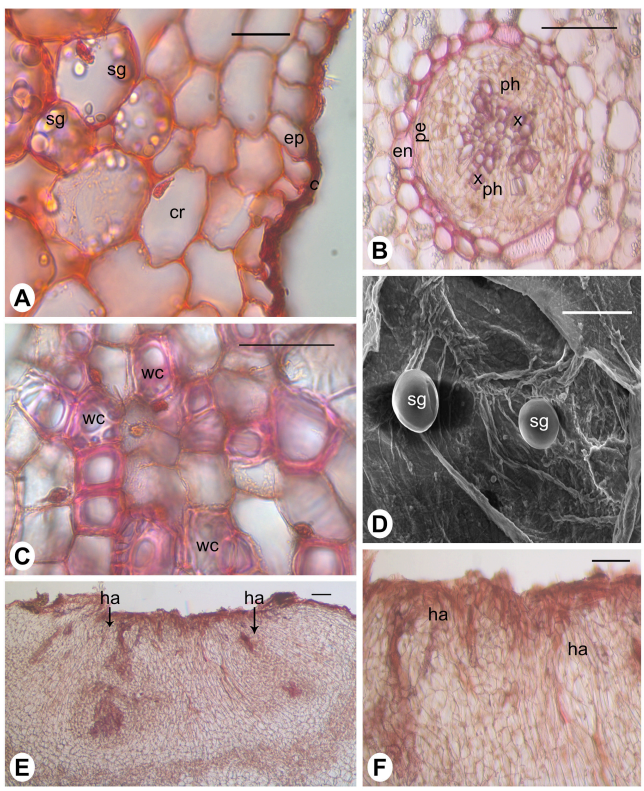

Figure 4. Transverse section of *Christisonia tubulosa* root showing thick-walled epidermis (ep), cortex (cr), and starch grains (sg) covered by cuticle (c) (A); xylem (x) and phloem (ph) covered by endodermis (en) and pericycle (pe) in stelar region (B); water-storage cell (wc) (C); scanning electron microscopic view of starch grains (sg) present in cortical layer (D); enlarged and magnified view of haustoria (ha) (E and F). Scale bars = 50 µm.

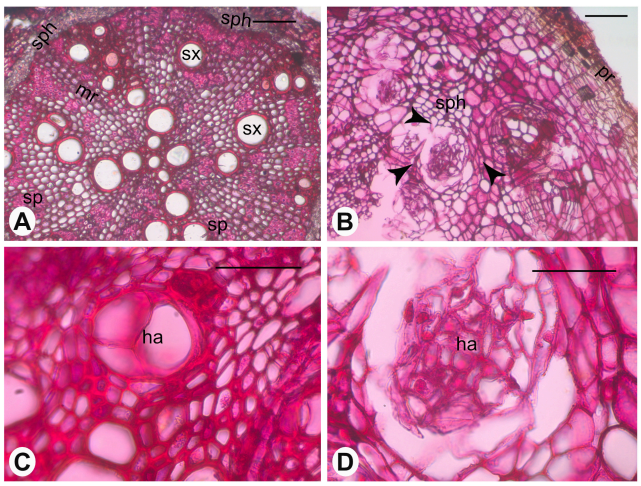

Figure 5. Infected root portion of the host plant, *Oreocnide integrifolia*, associated with *Christisonia tubulosa* haustoria. Transverse section of uninfected root of *O. integrifolia* (A); infected root showing haustorium (black arrow heads) of *C. tubulosa* (B-D); magnified view of the infected region of *C. tubulosa* root. Sph: secondary phloem; sx: secondary xylem; mr: medullary rays; sp: sclerenchymatous patches; pr: periderm; ha: haustoria. Scale bars = 50 µm.

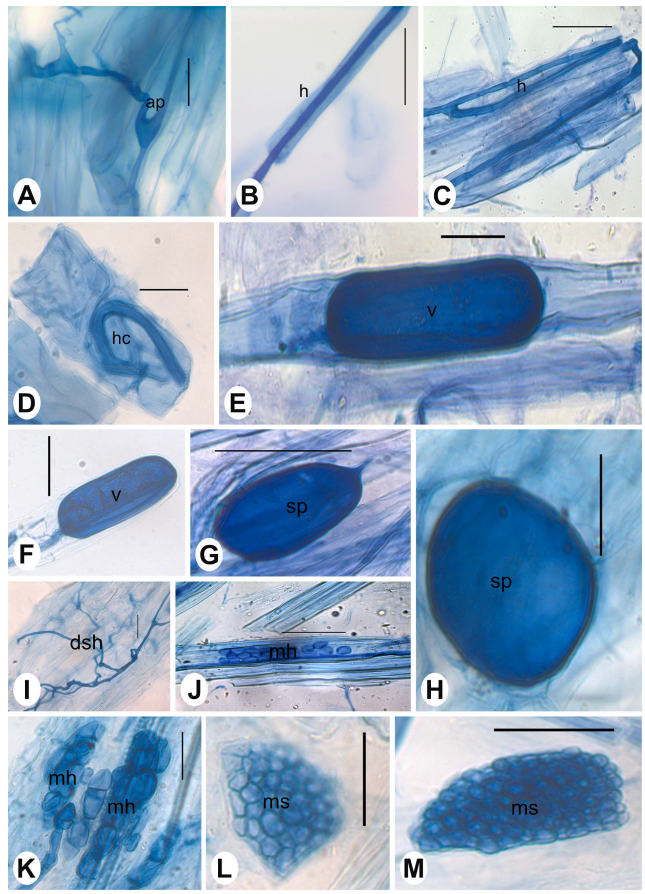

Figure 6. Root-associated fungal structures in *Christisonia tubulosa*. Arbuscular mycorrhiza (AM)-like appressorium (ap) on the root surface (A); hyphae (h) (B and C); hyphal coils (hc) in cortical cells (D); vesicle-like structures (v) in the root cortex (E and F); spores (sp) (G and H); dark septate fungal hyphae (dsh) (I); moniliform hyphae (mh) (J and K); microsclerotia (ms) (L and M). Scale bars = 50 µm.

also observed in the examined root samples (Fig. 6). The assessment of colonization using the magnified intersection method revealed that all root colonization parameters including percentage of root length with hyphae (%RLH), hyphal coils (%RLHC), vesicles (%RLV), total colonization (%TAM), dark septate hyphae (%RLDSH), moniliform hyphae (%RLMH), microsclerotia (%RLMS), and total dark septate endophytic (%TDSE) fungi varied significantly ($P < 0.05$). The percentage of root length with hyphae was 18.09 ± 0.43%, while hyphal coils were 12.73 ± 1.64% of the root length (Fig. 7). Similarly, %RLV occupied 6.12 ± 1.37% (Fig. 7) and %RLDSH were 7.55 ± 2.06% (Fig. 8). Likewise, %RLMH and %RLMS were 12.56 ± 2.41% and 19.46 ± 2.74% (Fig. 8). Overall, %TAM and %TDSE were 36.94 ± 0.62% and 39.57 ± 2.85%, respectively (Fig. 7 and 8).

Discussion

Christisonia tubulosa exhibits specialized anatomical traits characteristic of Orobanchaceae, including a structurally complex scape and a modified root system (Qasem 2022). The distinct tissue zones, reduced vascular complexity, and observed fungal colonization may represent adaptations associated with host dependence and growth in humid forest-floor habitats. These features are consistent with patterns reported in parasitic angiosperms (Schneeweiss 2013; Schweingruber et al. 2020; Westwood et al. 2010). Although Orobanchaceae have been studied extensively, anatomical information of this family remain limited. Existing research on *Christisonia* has focused primarily on taxonomy and morphology. The present study therefore provides a modern anatomical description of the scape, root, and rootstock, together with morphological documentation of root-associated fungal structures.

The scape exhibited a compact epidermal layer, that protect against desiccation and pathogen invasion, while the absence of a clearly defined exodermis may reflect an evolutionary reduction associated with the plant's dependence on its host for water and mineral acquisition (Schweingruber et al. 2020). Beneath the hypodermis, thick-walled sclerenchymatous fibres provides structural reinforcement, ensuring mechanical stability despite the lack of lignified secondary growth, a pattern consistent with the anatomical organization reported in *Orobanche aegyptiaca* Pers., where the non-cuticularized epidermis serves as the primary stress (Khan et al. 2009; Těšitel 2016). In addition, the xylem adapted for, haustorial

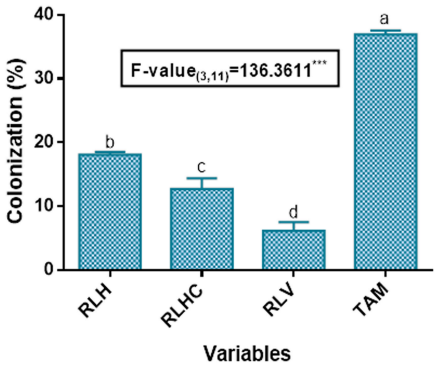

Figure 7. Extent of Arbuscular mycorrhizal (AM)-like fungal colonization in the root of *Christisonia tubulosa*. RLH: root length with hyphae; RLHC: root length with hyphal coils; RLV: root length with vesicles; TAM: total AM-like fungal colonization. Error bars indicate ± 1 standard error. Subscripts following F indicate degrees of freedom. *** P < 0.001. Bars for a fungal variable bearing the same letters are not significantly different according to Duncan's Multiple Range Test (P > 0.05).

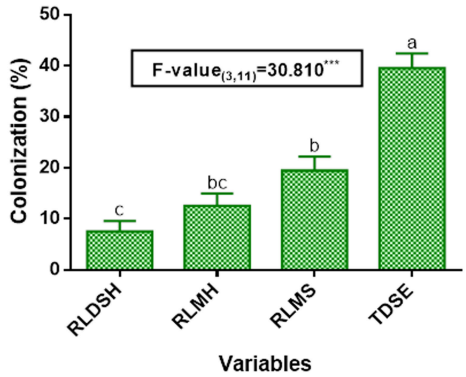

Figure 8. Extent of dark septate endophyte fungal colonization in the root of *Christisonia tubulosa*. RLDSH: root length with dark septate hyphae; RLMH: root length with moniliform hyphae; RLMS: root length with microsclerotia; TDSE: total root length with dark septate endophyte fungal structures. Error bars indicate ± 1 standard error. Subscripts following F indicate degrees of freedom. *** P < 0.001. Bars for a fungal variable bearing the same letters are not significantly different according to Duncan's Multiple Range Test (P > 0.05).

nutrient transfer instead of autonomous transport functions typical of autotrophic plants (Akbulut et al. 2016). Complementing this mechanism, phloem unloading in *Phelipanche ramosa* (L.) Pomel occurs predominantly within storage parenchyma, with sucrose transporters localized in cortical and medullary tissues, highlighting efficient internal redistribution of host-derived assimilates (Péron et al. 2017). Furthermore, the presence of prominent water-storage cells within the scape represents an important adaptive feature in holoparasitic taxa, facilitating osmotic regulation during periods of limited host connectivity (Zhang 2023). Consistent with these storage functions, abundant starch granules in the scape cortex serve as temporary carbohydrate reserves, sustaining metabolism when the host is unavailing during developmental transitions (Těšitel 2016). This storage role is further supported by similar observations in *Escobedia grandiflora* (L.f.) Kuntze, where starch accumulation provides critical reserves for reproductive development (Medina et al. 2019), and in *Orobanche picridis* F.W. Schultz, where secretory parenchyma cells containing large starch-filled plastids indicate that carbohydrate storage is a conserved family-level trait supporting energy-intensive parasitic growth and reproduction (Konarska and Chmielewski 2020).

The *C. tubulosa* rootstock appears intermediate between scape and root and may contribute to vegetative persistence and host attachment (Nickrent 2020). The compact epidermis and parenchymatous ground tissue protect internal tissues and may facilitate storage and movement of nutrients within the rootstock (Furuta et al. 2021). Sclerenchymatous fibres and water-storage cells may also contribute to mechanical support and tolerance of moisture fluctuation (Schneeweiss 2013). The vascular tissue, embedded in the ground tissue and containing small xylem elements, is reduced but remains structurally evident (Masumoto et al. 2021). This agrees with observations that xylem development in subterranean organs of parasitic plants is often limited, as water and solute transport relies mainly on haustorial connections to the host rather than on extensive intrinsic vascular networks (Wakatake et al. 2020). The parenchymatous cortex also contains raphides, needle-shaped calcium oxalate crystals, together with water-storage cells, which may contribute to mechanical support, defence, and calcium regulation (Lawrie et al. 2023).

The root hairs are absent in the roots of holoparasitic plants, as absorption occurs through haustoria (Irving and Cameron 2009). Consistent with this specialization, the root structure in *C. tubulosa* exhibited a lack of root hairs and a clear radial organization with distinct outer and inner tissues, resembling the compact peripheral regions, broad cortical parenchyma, and well-defined stele as reported in *Orobanche aegyptiaca* Pers. (Khan et al. 2009). This structural differentiation also supports anchorage, storage, and early host interaction, reflecting adaptations in parasitic taxa that maintain soil contact before haustorial establishment (Westwood et al. 2010). The presence of a thick-walled, uniseriate epidermis with occasional passage cells is a notable feature in parasitic plants of Orobanchaceae. The cortex and sclerenchymatous fibre development in *C. tubulosa* support dual functions, such as mechanical support and the accommodation of fungal partners in the rhizosphere (Yoshida et al. 2016). In addition, the cortex and associated sclerenchymatous fibres provide both mechanical support and a conducive environment for rhizosphere interactions,

including associations with beneficial microorganisms (Yoshida et al. 2016). The endodermis also forms a prominent structural barrier between the cortex and stele, reflecting specialized differentiation linked to haustorium-related vascular modifications observed in Orobanchaceae (Pérez-de-Luque et al. 2005). Recent studies indicate that endodermal thickening in parasitic roots acts as a protective barrier, regulating radial transport and reducing water loss and pathogen entry under variable soil conditions (Holbein et al. 2019). Correspondingly, the distinction between the endodermis and pericycle indicates developmental plasticity, facilitating tissue reorganization necessary for host vascular integration (Furuta et al. 2021). In line with these anatomical modifications, the compact arrangement of small xylem elements reflects a hydraulically efficient and embolism-resistant architecture suited to fluctuating water availability (Al-Joboury and Aliwy 2021). A similar vascular arrangement has been documented in *Phelipanche ramose* (L.) Pomel, where resource acquisition depends primarily on haustorial connections rather than extensive autonomous transport systems (Le Corre et al. 2023). This dependence is further supported by observations in *Phelipanche aegyptiaca* (Pers.) Pomel, where the prehaustorium originates from the embryonic root and establishes direct vascular continuity with the host through specialized xylem bridges (Hu et al. 2025). The occurrence of water-storage cells adjacent to vascular tissues represents an additional adaptive feature. Recent work has demonstrated that parasitic plants frequently rely on internal water buffering to sustain metabolism when the host resource flow is inconsistent or temporarily disrupted (Mutuku et al. 2021). Such storage tissues, in combination with starch-rich parenchyma, enhance physiological resilience and support sustained parasitic growth. Zhou et al. (2021) reported that hemiparasitic plants accumulate starch-rich parenchyma as an assimilate storage strategy, providing energy reserves during limited host connectivity or stress; a similar mechanism is suggested by the starch-rich tissues observed in *C. tubulosa*, which supports survival and haustorium function.

The present investigation revealed AM-like and DSE-like fungal structures in the roots of *C. tubulosa*. Typical *Arum*-type arbuscules or arbusculate coils were not observed in the examined root specimens. Therefore, the structures recorded here should be interpreted cautiously as morphological evidence of root-associated fungal colonization rather than as proof of a functional AM symbiosis. The presence of hyphal coils, vesicle-like structures, septate melanized hyphae, moniliform hyphae, and microsclerotia suggests that *C. tubulosa* roots can harbour diverse fungal structures, including forms resembling AM and DSE colonization. AM and DSE fungi can colonize a wide range of plant species, and extraradical hyphae may connect roots of different plants through common fungal networks (Rillig et al. 2025), but such interactions were not directly tested in the present study. Accordingly, any role of these fungi in resource acquisition or host-parasite interactions remains hypothetical and should be examined by molecular and functional approaches. The observed variation among colonization variables suggests that fungal structures are not distributed uniformly along the roots. Similar heterogeneity has been reported in other systems, where environmental and host factors influence the spatial distribution of fungal structures (Grünfeld et al. 2022). Overall, the anatomical features and fungal structures documented in *C. tubulosa* contribute to the understanding of this holoparasitic plant and its belowground associations, while their functional significance requires further study.

Conclusion

This study provides a modern anatomical description of *C. tubulosa* and documents root-associated fungal structures in a population from the Western Ghats. The vegetative organs showed features consistent with a holoparasitic lifestyle, including reduced absorptive structures, storage tissues, and haustorial attachment to the host root. Morphological observations also revealed AM-like and DSE-like fungal structures in the roots. These findings provide baseline information for future anatomical, ecological, and conservation-oriented studies of this rare species. However, the results should be interpreted in light of several limitations. The anatomical observations and assessments of fungal colonization were based on samples collected from a single site and a limited number of individuals. Fungal taxa were identified morphologically, not molecularly, precluding definitive taxonomic or functional assignment. Proposed adaptive roles of anatomical structures remain speculative without experimental testing, and the ecological significance of fungal colonization requires physiological, molecular, and functional validation.

References

Akbulut MK, Akçin ÖE, Şenel G (2016) Anatomical and micromorphological properties of holoparasite *Orobanche gracilis* and *Orobanche fuliginosa* (Orobanchaceae) species. Rend Fis Acc Lincei 27:565-571.

Al-Joboury KR, Aliwy SA (2021) Morphological and anatomical study in some species of *Orobanche*. J Biotechnol Res Center 15:25-30.

Baskin JM, Baskin CC (2022) Germination and seed/embryo size in holoparasitic flowering plants with “dust seeds” and an undifferentiated embryo. Bot Rev 88:1-49.

Bennett JR, Mathews S (2006) Phylogeny of the parasitic plant family Orobanchaceae inferred from phytochrome A. Am J Bot 93:1039-1051.

Brundrett MC (2011) Commentary on the de Vega et al. (2010) paper on hyphae in the parasitic plant *Cytinus*: Mycorrhizal fungi growing within plants are not always mycorrhizal. Am J Bot 98:595-596.

Casadesús A, Munné-Bosch S (2021) Holoparasitic plant-host interactions and their impact on Mediterranean ecosystems. Plant Physiol 185:1325-1338.

Chaudhary A, Poudyal S, Kaundal A (2025) Role of arbuscular mycorrhizal fungi in maintaining sustainable agroecosystems. Appl Microbiol 5:6.

Dastjerdi MAB, Yousefi AR, Jamshidi K, Pouryousef M, Amanifar S (2025) Inoculation with *Talaromyces trachyspermus* and arbuscular mycorrhizal fungus alongside sulfonylurea herbicides alters *Orobanche aegyptiaca* and tomato growth. Sci Rep 15:27184.

De Vega C, Arista M, Ortiz PL, Talavera S (2010) Anatomical relations among endophytic holoparasitic angiosperms, autotrophic host plants and mycorrhizal fungi: a novel tripartite interaction. Am J Bot 97:730-737.

Furuta KM, Xiang L, Cui S, Yoshida S (2021) Molecular dissection of haustorium development in Orobanchaceae parasitic plants. Plant Physiol 186:1424-1434.

Goyet V, Wada S, Cui S, Wakatake T, Shirasu K, Montiel G, Simier P, Yoshida S (2019) Haustorium inducing factors for parasitic Orobanchaceae. Front Plant Sci 10:1056.

Grünfeld L, Skias G, Rillig MC, Veresoglou SD (2022) Arbuscular mycorrhizal root colonization depends on the spatial distribution of the host plants. Mycorrhiza 32:387-395.

Holbein J, Franke RB, Marhavý P, Fujita S, Górecka M, Sobczak M, Geldner N, Schreiber L, Grundler FM, Siddique S (2019) Root endodermal barrier system contributes to defence against plant-parasitic cyst and root-knot nematodes. Plant J 100:221-236.

Hu X, Cao X, Zhang L, Zhao Q, Zeng X, Wei Y, Han Y, Lin P, Li Y, Yao Z, Zhao S (2025) 6-Hydroxynicotinic acid from *Cucumis melo* inhibits prehaustorium formation in *Phelipanche aegyptiaca* via disruption of auxin signalling pathway. Mol Plant Pathol 26:e70137.

Ikeda H, Fukuda T, Yokoyama J (2016) Endophytic fungi associated with a holoparasitic plant, *Balanophora japonica* (Balanophoraceae). Am J Plant Sci 7:152-158.

Irving L J, Cameron DD (2009) You are what you eat: interactions between root parasitic plants and their hosts. Adv Bot Res 50:87-138.

Jose Mathew JM, George KV (2015) *Christisonia mira* (Orobanchaceae): a new plant species from Southern Western Ghats, India. Telopea 18:425-431.

Kanivalan I, Rajendran A (2022) A new species *Christisonia rarissima* (Orobanchaceae) from the Southern Western Ghats of India. Nord J Bot 10:e03686.

Khan MA, Sharif T, Ahmad M, Zafar M, Tareen RB (2009) Anatomical characterization of parasitic plants of Pakistan. Pak J Bot 41:2661-2669.

Konarska A, Chmielewski P (2020) Taxonomic traits in the microstructure of flowers of parasitic *Orobanche picridis* with particular emphasis on secretory structures. Protoplasma 257:299-317.

Koske RE, Gemma JN (1989) A modified procedure for staining roots to detect VA mycorrhizas. Mycol Res 92:486-488.

Lawrie NS, Cuetos NM, Sini F, Salam GA, Ding H, Vancolen A, Nelson JM, Erkens RH, Perversi G (2023) Systematic review on raphide morphotype calcium oxalate crystals in angiosperms. AoB Plants 15:1-16.

Le Corre V, Reibel C, Kati V, Gibot-Leclerc S (2023) Host-associated genetic differentiation and origin of a recent host shift in the generalist parasitic weed *Phelipanche ramosa*. Ecol Evol 13:e10529.

Masumoto N, Suzuki Y, Cui S, Wakazaki M, Sato M, Kumaishi K, Shibata A, Furuta KM, Ichihashi Y, Shirasu K, Toyooka K, Yoshida S (2021) Three-dimensional reconstructions of haustoria in two parasitic plant species in the Orobanchaceae. Plant Physiol 185:1429-1442.

Mathew J, Salim PM (2022) *Christisonia flavirubens* (Orobanchaceae), a new species from south Western Ghats, India. Biodivers Res Conserv 68:1-7.

McGonigle TP, Miller MH, Evans DG, Fairchild GL, Swan JA (1990) A new method which gives an objective measure of colonization of roots by vesicular arbuscular mycorrhizal fungi. New Phytol 115:495-501.

McNeal JR, Bennett JR, Wolfe AD, Mathews S (2013) Phylogeny and origins of holoparasitism in Orobanchaceae. Am J Bot 100:971-983.

Medina EC, Santos M, Nodari RO (2019) Post-seminal structure and development of the hemiparasitic plant *Escobedia grandiflora* (Orobanchaceae). Acta Sci Biol Sci 41:1-8.

Molina J, de Guzman RC, Wicaksono A, Muth T, Pedales R, Diaz D, Kusuma AB, Li C, Margolis H, Karnitskiy F, Estopace A, Pell S (2024) The endophyte’s endophytes: the microbial partners of the endangered plant parasite *Rafflesia speciosa* (Rafflesiaceae) reveal clues about its cryptic biology and cues for cultivation. J Plant Interact 19:2304221.

Mutuku JM, Cui S, Yoshida S, Shirasu K (2021) Orobanchaceae parasite–host interactions. New Phytol 230:46-59.

Nickrent DL (2020) Parasitic angiosperms: how often and how many? Taxon 69:5-27.

Pérez-de-luque A, Rubiales D, Cubero JI, Press MC, Scholes J, Yoneyama K, Takeuchi Y, Plakhine D, Joel DM (2005) Interaction between *Orobanche crenata* and its host legumes: unsuccessful haustorial penetration and necrosis of the developing parasite. Ann Bot 95:935-942.

Péron T, Candat A, Montiel G, Veronesi C, Macherel D, Delavault P, Simier P (2017) New insights into phloem unloading and expression of sucrose transporters in vegetative sinks of the parasitic plant *Phelipanche ramosa* L. (Pomel). Front Plant Sci 7:2048.

POWO (2025) Plants of the World Online. Royal Botanic Gardens, Kew. http://www.plantsoftheworldonline.org/

Qasem JRS (2022) Parasitic Weeds of Jordan: Species, Hosts, Distribution and Management. Part 1: Root Parasites; Orobanchaceae, Santalaceae, and Cynomoriaceae. Bentham Science Publishers. 1-82.

Rillig MC, Lehmann A, Lanfranco L, Caruso T, Johnson D (2025) Clarifying the definition of common mycorrhizal networks. Funct Ecol 39:1411-1417.

Ruotsalainen AL, Kauppinen M, Wäli PR, Saikkonen K, Helander M, Tuomi J (2022) Dark septate endophytes: mutualism from by-products? Trends Plant Sci 27:247-254.

Schneeweiss GM (2013) Phylogenetic relationships and evolutionary trends in Orobanchaceae. In Joel D, Gressel J, Musselman L, Eds., Parasitic Orobanchaceae: Parasitic Mechanisms and Control Sstrategies. Springer, Berlin, Heidelberg, 243-265.

Schweingruber FH, Dvorský M, Börner A, Doležal J (2020) Orobanchaceae. In Schweingruber FH, Dvorský M, Börner A, Doležal J, Eds., Atlas of Stem Anatomy of Arctic and Alpine Plants Around the Globe. Cham: Springer International Publishing, 223-233.

Smith SE, Read DJ (2010) Mycorrhizal Symbiosis. Academic Press, London.

Těšitel J (2016) Functional biology of parasitic plants: a review. Plant Ecol Evol 149:5-20.

Thazhe Arunraj P, Natarajakaimal Sanjai V, Mathew J (2025) Notes on the taxonomy and parasitism of *Christisonia tubulosa* (Orobanchaceae). Nord J Bot 4:e04417.

van Der Ent A, Wong KM (2015) Range extension of *Christisonia scortechinii* from mainland Southeast Asia into Borneo, and notes on the distinction between *Aeginetia* and *Christisonia* (Orobanchaceae). Bot Stud 56:28.

Wakatake T, Ogawa S, Yoshida S, Shirasu K (2020) An auxin transport network underlies xylem bridge formation between the hemi-parasitic plant *Phtheirospermum japonicum* and host *Arabidopsis*. Development 147: dev187781.

Westwood JH, Yoder JI, Timko MP, Depamphilis CW (2010) The evolution of parasitism in plants. Trends Plant Sci 15:227-235.

Worsdell WC (1895) On the comparative anatomy of certain species of the genus *Christisonia*. Ann Bot 9:103-136.

Wu C, Wang W, Wang X, Shahid H, Yang Y, Wang Y, Wang S, Shan T (2022) Diversity and communities of culturable endophytic fungi from the root holoparasite *Balanophora polyandra* Griff. and their antibacterial and antioxidant activities. Ann Microbiol 72:19.

Yoshida S, Cui S, Ichihashi Y, Shirasu K (2016) The haustorium, a specialized invasive organ in parasitic plants. Annu Rev Plant Biol 67:643-667.

Zhang X (2023) Effects of nutrient conditions on haustorium formation on parasitic plants in Orobanchaceae. PhD Thesis. Nara Institute of Science and Technology, Nara, Japan.

Zhou XR, Zhang NN, Zhao YM, Dai L, Xu DP, Xu GF, Tian J (2021) Distribution dynamics and roles of starch in non-photosynthetic vegetative organs of *Santalum album* Linn., a hemiparasitic tree. Front Plant Sci11:532537.